Frequency Shifts in SERS for Biosensing

Kiang Wei Kho,[†,‡,§,⊥] U. S. Dinish,[§] Anil Kumar,[∥] and Malini Olivo[‡,§,⊥,#,*]

[†]The Blackett Laboratory, Imperial College London, Prince Consort Road, London, U.K., [‡]School of Physics, National University Ireland, University Road, Galway, Ireland, [§]Bio-Optical Imaging Group, Singapore Bioimaging Consortium, Agency for Science Technology and Research (A*STAR), 11 Biopolis Way, #02-02 Helios, Singapore 138667, [⊥]National Cancer Centre, Division of Medical Sciences, 11 Hospital Drive, Singapore 169610, [∥]Singapore Immunology Network, Agency for Science Technology and Research (A*STAR), 8A Biomedical Grove, Level 3 Lab Module 9, Immunos, Singapore 138648, and [#]Department of Pharmacy, Faculty of Science, National University of Singapore, 18 Science Drive 4, Singapore 117543

ABSTRACT

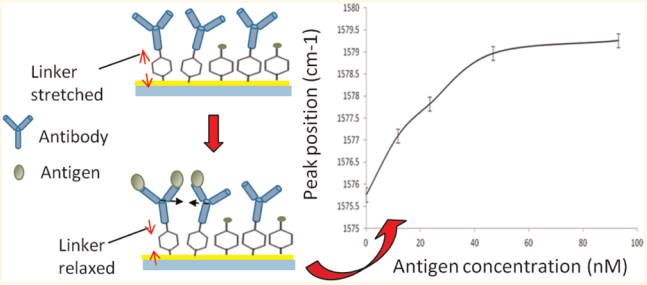

We report an observation of a peculiar effect in which the vibrational frequencies of antibody-conjugated SERS-active reporter molecules are shifted in quantitative correlation with the concentration of the targeted antigen. We attribute the frequency shifts to mechanical perturbations in the antibody–reporter complex, as a result of antibody–antigen interaction forces. Our observation thus demonstrates the potentiality of an antibody-conjugated SERS-active reporter complex as a SERS-active nanomechanical sensor for biodetection. Remarkably, our sensing scheme, despite employing only one antibody, was found to be able to achieve detection sensitivity comparable to that of a conventional sandwich immunoassay. Additionally, we have carried out a proof-of-concept study into using multiple "stress-sensitive" SERS reporters for multiplexed detection of antigen–antibody bindings at the subdiffraction limit. The current work could therefore pave the way to realizing a label-free high-density protein nanoarray.

KEYWORDS: stress · sensor · SERS · protein · frequency shift · label-free biodetection

One of the milestones in molecular biology is the completion of the genome project, which has brought about a better understanding of cellular functions and disease development at the molecular level. This has subsequently led to various clinical applications, ranging from the detection of chromosomal abnormalities to gene therapy.[1] Despite such breakthroughs, the measurements of gene expression levels alone, though informative, do not provide complete insight into the function of a biological system.[1] This is due primarily to the fact that most cellular activities are regulated by gene products, *i.e.*, proteins.[2] Recent studies into the proteome have not only revealed the far more complex network of protein signaling[2] but also exposed the potentiality of proteins as molecular markers.[3] It is thus anticipated that a multiplexed platform capable of probing the expression levels of a large panel of proteins simultaneously could contribute significantly to both the research-based diagnosis and the clinical-based diagnosis.[4−6]

While DNA microarrays have enjoyed many successes, the development of a protein array on the other hand has been plagued by many challenges, due mainly to the high diversity of proteins.[1] This implies that a protein array must bear an even greater number of biofeatures compared to its DNA counterpart,[1] which could unfortunately and inevitably compromise the overall detection sensitivity, in the sense that larger sample volumes are now required. Additionally, the microsize biofeatures will lead to impractically long incubation times (of up to 18 h) caused by the limited "mass transport" dynamics.[7−10] A solution proposed for these issues is to pack as many biofeatures as possible within a small area on the array through the use of a high-resolution lithographic method such as dip-pen lithography,[11] inkjet and pipet deposition,[12] and nanocontact printing.[13,14] However, despite these developments, the potentiality of a high-density nanoarray is still compromised by the lack of a suitable optical readout system, since the feature sizes are well below the diffraction limit. Although the technique of atomic-force microscope (AFM) has been suggested as an alternative, as demonstrated by Jaschke and Butt,[15] such a serial process is generally slow as well as highly demanding in the overall system design.

In this paper, we propose a novel readout method based on our observation that the Raman frequencies of an antibody-conjugated SERS-active molecule can be affected when binding it to its targeted antigen. The

* Address correspondence to Malini_olivo@sbic.a-star.edu.sg.

Received for review January 24, 2012 and accepted May 29, 2012.

Published online May 29, 2012
10.1021/nn300352b

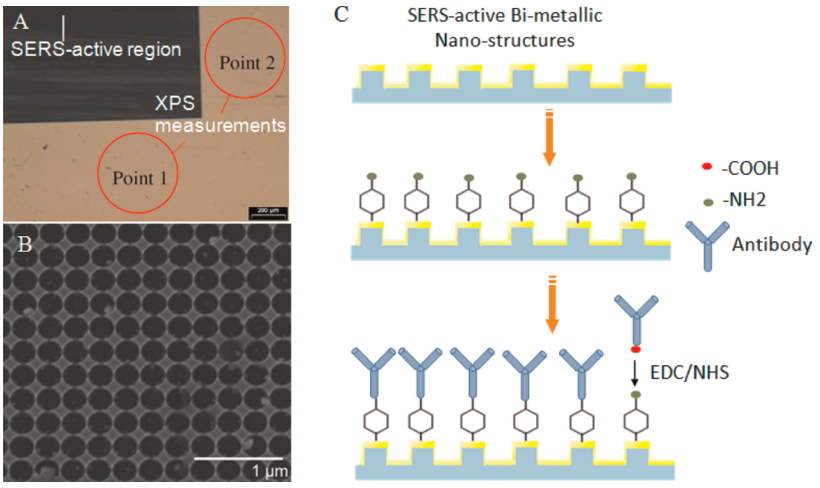

Figure 1. Fabrication scheme. (A) Microscopic image of the nanopatterned substrate, showing the dark SERS-active region and the smooth reflective Au surface on which XPS measurements (points 1 and 2) were carried out. (B) Field-emission scanning-electron microscope image of the SERS-active nanostructured region. (C) Functionalization of a Au/Ag bimetallic nanostructure with anti-H1/4-ATP.

observed frequency shifts were attributed to structural deformations in the antibody-conjugated SERS reporter molecule as a result of the binding event. In other words, a single antibody-conjugated SERS reporter molecule could behave as a nanomechanical bio sensor. As such, our method permits detection of antibody−antigen bindings without the use of a secondary antibody, *i.e.*, label-free detection;, in great contrast to previously proposed SERS immunoassay schemes, which require two antibodies for each antigen. Additionally, owing to the high spectral multiplexicity of SERS, individual binding events in subdiffraction biofeatures can now be detected by resolving the Raman spectra emanated from the corresponding "stress sensors". To illustrate this point, we show simultaneous measurements of multiple binding events within one single laser spot (~1 μm). While microcantilevers have previously been utilized to measure reaction forces between biomolecules,[16] we stress that our approach is relatively more amendable for miniaturization since subdiffraction patterning of antibody-conjugated SERS reporters can be easily accomplished using existing nanolithography techniques. Finally, unlike the serial approach of AFM−readout, the current scheme allows parallel measurements of multiple antibody-conjugated SERS reporters owing to their spectral distinguishability. This is in great contrast to the LSPR (localized surface plasmon resonance) sensors, where mutltiplexed detections can become difficult to achieve at the subdiffraction level.[17] To the best of our knowledge, our study is the first demonstration of multiplexed label-free detection of proteins using a nano stress-sensor concept in a SERS-detection mode.

RESULTS AND DISCUSSION

Conjugating Antibody to SERS-Active Reporters. In the current study, we concentrate primarily on phenol- and purine-based SERS reporter molecules. We begin by investigating the SERS response of anti-influenza-H1 (anti-H1)-conjugated 4-aminothiophenol (anti-H1/4-ATP) to mechanical stresses induced upon binding to the influenza-H1 (H1) antigen. This is achieved by first coating a self-assembled monolayer (SAM) of 4-ATP on a SERS-active bimetallic Au/Ag surface produced by deep-UV (DUV) lithography, as depicted in Figure 1. Immobilization of anti-H1, the capturing antibody, was realized by first activating the carboxyl terminal of the crystal segment with 1-ethyl-3-(3-dimethylaminopropyl)carbodiimide (EDC)/*N*-hydroxysuccinimide (NHS) and then reacting with the amino group of the 4-ATP. This ensures that the antibody is oriented preferentially in the "upright" position, thereby allowing for access to its binding sites. The surface functionalization was confirmed by X-ray photoelectron spectroscopy (XPS),[18] as described in ref 18, performed at a photoelectron takeoff angle of 90° with a monochromatic Al K-alpha source (1486.6 eV) as shown in Table 1. Note that, in order to prevent any artifact that could potentially arise from the SERS-active nanostructures, XPS spectra were instead collected from the smooth Au area (700 μm × 700 μm) beside the SERS-active region on the sample

TABLE 1. Relative Surface Composition of Various Surfaces

	Au surface[a]	4-ATP-Au[b]	anti-H1/4-ATP-Au[c]
Au	65.5%	9%	5%
C	27.9%	47.2%	63%
N		2.3%	6.7%
O	6.6%	13.9%	13.9%
S		8.1%	6.6%

[a] Smooth, unmodified Au surface. [b] 4-ATP-coated Au surface. [c] Anti-H1 covalently attached to 4-ATP-coated Au surface.

(points 1 and 2 in Figure 1A). Since this particular area was also similarly modified, the corresponding XPS data were used to infer the functionalization conditions on the nanostructures. 4-ATP functionality was evidenced from the increased carbon and oxygen composition as compared to the plain Au surface (see Table 1). Anti-H1 immobilization was evidenced from the further increase in the carbon/oxygen ratios as well as in the nitrogen content. Surface coverage of anti-H1 is also apparent from the diminishing sulfur XPS signal arising from the initial 4-ATP layer.

SERS Responses. To improve the binding specificity (*i.e.*, to reduce nonspecific bindings), the anti-H1/4-ATP layer was blocked with 0.1 mM glycine. The response of the anti-H1/4-ATP to binding events was studied by exposing it to solutions of H1 prepared at different concentrations in PBS. Reaction time was kept at 10 min for all reactions. Figure 2a shows the SERS spectra of the anti-H1/4-ATP as a function of H1 concentrations varying from 0 to 93 nM. Peak assignments are shown in Table 2 as acquired from Hong *et al.*[18] The most prominent Stokes bands in the spectra occur at 1080, 1144, 1389, and 1436 cm^{-1} and at 1572−1586 cm^{-1}, which are assignable to either a_1 or b_2 species in-plane vibration modes of the benzene ring.[19] Of these, peaks around 1080 and 1580 cm^{-1}, which correspond to the C−S stretching and C−C breathing modes, respectively, are particularly responsive to the antibody−antigen binding. In fact, under a higher spectral resolution of 0.1 cm^{-1} (obtained with 1800 L/mm grating), we found, by virtue of curve-fitting, that as the H1 concentration increases, these bands (see Figure 2b−e) are upshifted in a manner characterized by a first-order antigen−antibody binding isotherm, as shown in Figure 2d and e.[20] In order to ensure the response indeed stems from binding of the antibody to its target antigen, a specificity test was carried out. This is shown in Figure 2f, in which the ability of anti-H1/4-ATP to distinguish between H1 and BSA (bovine serum albumin), both in an equal concentration of 1 μM, is evident. Taking into consideration the errors, we estimate, as per ref 20, the detection limit (DL) to be about 2.2 nM. For a comparison, Figure 2g shows the dose−response curve for anti-H1 as obtained with a conventional ELISA (see §1 in the Supporting Information (SI) for details). The DL for this assay is about 1 nM, with a saturation point at 40 nM.

Mechanical Explanation of the Observed Frequency Shifts. Since the antibody molecules are within reach of the plasmon fields, one may expect postbinding conformations (if any) in the antibody structure to contribute to the observed frequency shifts. However, such a possibility can be safely ruled out, for the fact that the antibody contributes only negligibly to the measured SERS spectra (see §2 in the SI). In addition, we can also rule out contributions from the bound antigen, since the epitope of the antibody is located about 10 nm (the size of the antibody molecule) away from the Au surface, which is significantly larger than the 3 nm decay length of the plasmon near-fields.[21] Therefore, the question to be confirmed is whether the observed peak shifts are simply a consequence of binding-induced variations in the local pH level experienced by the unconjugated 4-ATP molecules in the vicinity of the antibody-conjugated ones. To this end, we study the effect of H1 concentrations on the peak-intensity ratios between I_{1620}, which is indicative of the protonation state of the NH_2 group in unconjugated 4-ATP,[22] and I_{1007} (see Figure 3d). We then compare these data with the ratio I_{1620}/I_{1007} derived from the SERS spectra of pure 4-ATP SAMs (see Figure 3a) immersed in buffer solutions of different pH values (ranging between 5 and 9). More details relating to Figure 3a and d can be found in §3 of the SI.

A stark difference can be seen in the pH-induced changes in I_{1620}/I_{1007} measured from the 4-ATP SAM (Figure 3a), when compared with those (Figure 3d) corresponding to anti-H1/4-ATP. Whereas variation in the 4-ATP I_{1620}/I_{1007} is as much as 57.7%, corresponding ratio values from the anti-H1/4-ATP spectra, on the other hand, are relatively unaffected (∼1%) by the H1 concentration, thereby suggesting that H1−anti-H1 binding should not significantly alter the local pH value. We note that this is possible for two reasons: (a) the isoelectric point of the antibody IgG molecule is generally at pH 6−7.3, so at the current working pH of ∼7.0, the net magnitude of the positive and negative changes on the surface of the antibody should be approximately equal; that is, the antibody is neutral, regardless of its binding state;[23] (b) the binding sites of the anti-H1 antibody are about 10 nm away from its base at which it is anchored to the 4-ATP layer. Thus, the bound antigen could elicit only a minimal effect on the local pH seen by 4-ATP. It is therefore concluded that the binding-induced shifts in wavenumbers observed in Figure 2 are likely caused by factor other than pH. We postulate that mechanical perturbations to the 4-ATP linker in the conjugated anti-H1/4-ATP construct are responsible for the observed shifts. This is evident by the fact that neither the 1080 nor the 1580 cm^{-1} peak in the 4-ATP SERS spectra is sensitive to pH changes (see Figure 3b and c and also details in §3 of the SI). We have also ruled out the possibility that other postbinding chemical effects were responsible for the observed shifts. This is based on our previous studies that no binding-induced frequency shifts could be observed if the antibody and the reporter molecules were adsorbed separately onto the Au surface (*i.e.*, immobilized but not attached to each other).[24]

Further evidence that points to our mechanical theory can be derived by monitoring changes in the 1080 and 1580 cm^{-1} peak position when the antibody is covalently attached to the 4-ATP linker. This is shown

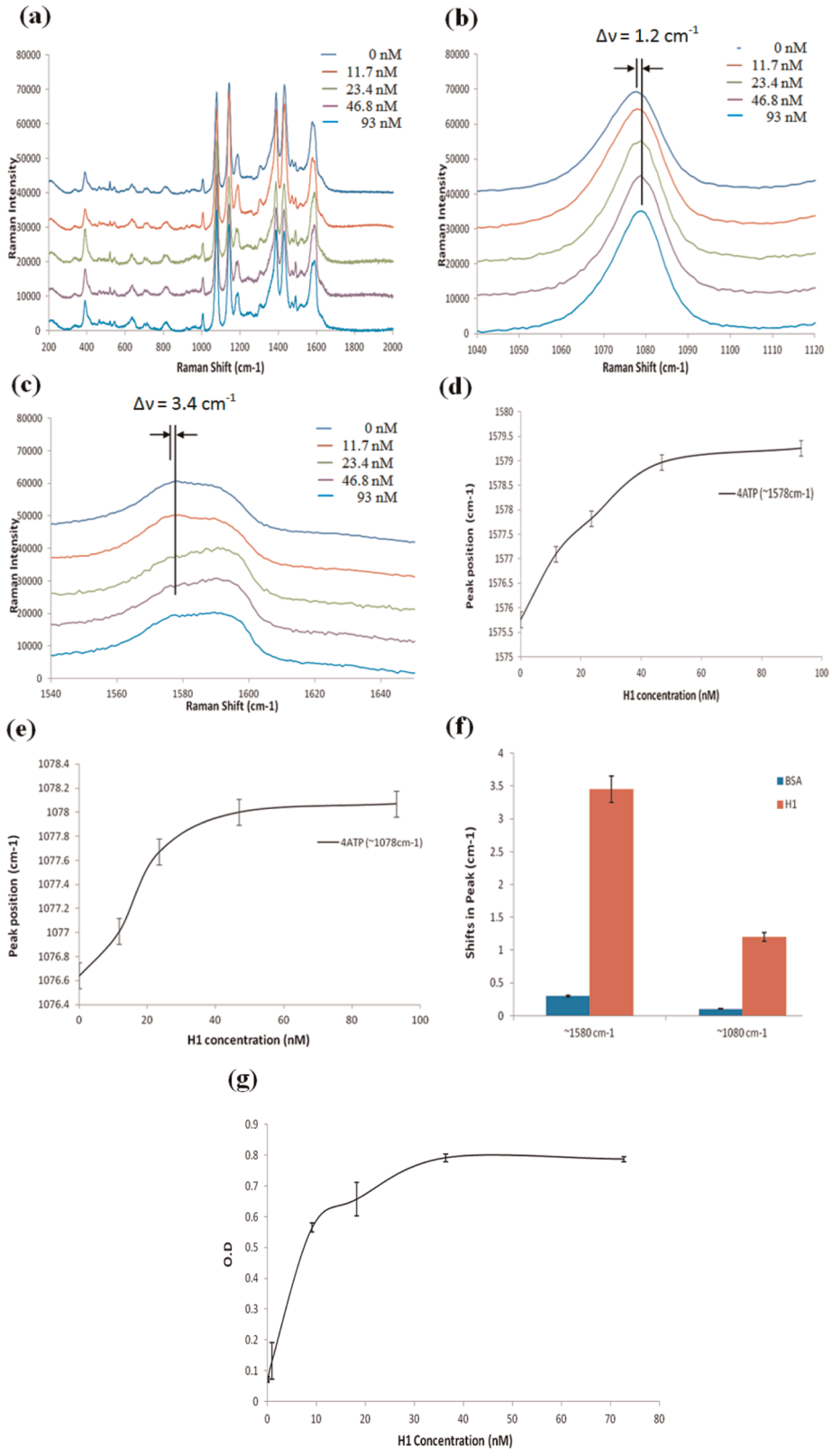

Figure 2. Responses of the anti-H1/4-ATP to H1 concentrations. (a) Average SERS spectra at different H1 concentrations. (b–e) Shifts in SERS peak position at around 1080 and 1580 cm^{-1} in response to the H1 binding. (f) Specific test showing selectivity of the two peaks. Error bars = 0.02%. (g) Dose–response curve for anti-H1 as obtained with ELISA. Note that, for clarity, SERS spectra shown in a–c have been offset vertically.

in Figure 3e and f. As can be seen, a significant down-shift in both peaks is observable following anti-H1 conjugation, signifying tensile deformation in the C–S bond (1080 cm^{-1}) as well as in the benzene ring

TABLE 2. Vibration Modes Observed by SERS Spectroscopy on a 4-ATP-Modified SERS Substrate[a]

wavenumber (cm^{-1})	vibrational assignment
1620	$\rho(NH_2)$
1586	ν(CC), 8a (a_1)
1580	ν(CC), 8a (b_2)
1505	$\rho(NH_2)$
1489	ν(CC) + δ(CH), 19a (a_1)
1427	ν(CC) + δ(CH), 19b (b_2)
1386	ρ(CH) + ν(CC), 3 (b_2)
1303	ν(CC) + δ(CH), 14 (b_2)
1179	δ(CH), 9a (a_1)
1141	δ(CH), 9b (b_2)
1081	ν(CS), 7a (a_1)
1007	γ(CCC) + γ(CC), 18a (a_1)
816	π(CH), 11 (b_1)
705	π(CS) + π(CH) + π(CC), 4 (b_1)
639	γ(CCC), 12 (a_1)

[a] ν: stretching; ρ: rocking; δ: bending. For ring vibrations, the corresponding vibrational modes of benzene and the symmetry species under C_{2v} symmetry are indicated.

(1580 cm^{-1}), as illustrated in Figure 4a, b. In fact, a similar observation of changes in the 1580 cm^{-1} peak toward a lower wavenumber was observed in poly(*p*-phenylenebenzobisoxazole) fiber under a tension load.[25] However, upon introducing H1 antigen, both the 1080 and the 1580 cm^{-1} peaks recover to their initial spectral positions, suggesting that the H1−anti-H1 binding leads to a relaxation of the stress within the 4-ATP (Figure 4b, c). While the exact origin of stresses induced when an adsorbent interacts with a funcitonalized surface is unclear at the current stage, and remains a debated topic,[26] here we invoke an explanation as outlined by Moulin *et al.*[23] It is possible that the initial stretching of the 4-ATP linker after the anti-H1 conjugation is caused by intermolecular repulsion between the immobilized antibodies owing to steric hindrance (shown as a dotted line in Figure 4). It would be instructive, at this point, to estimate the amount of energy required to generate tensile

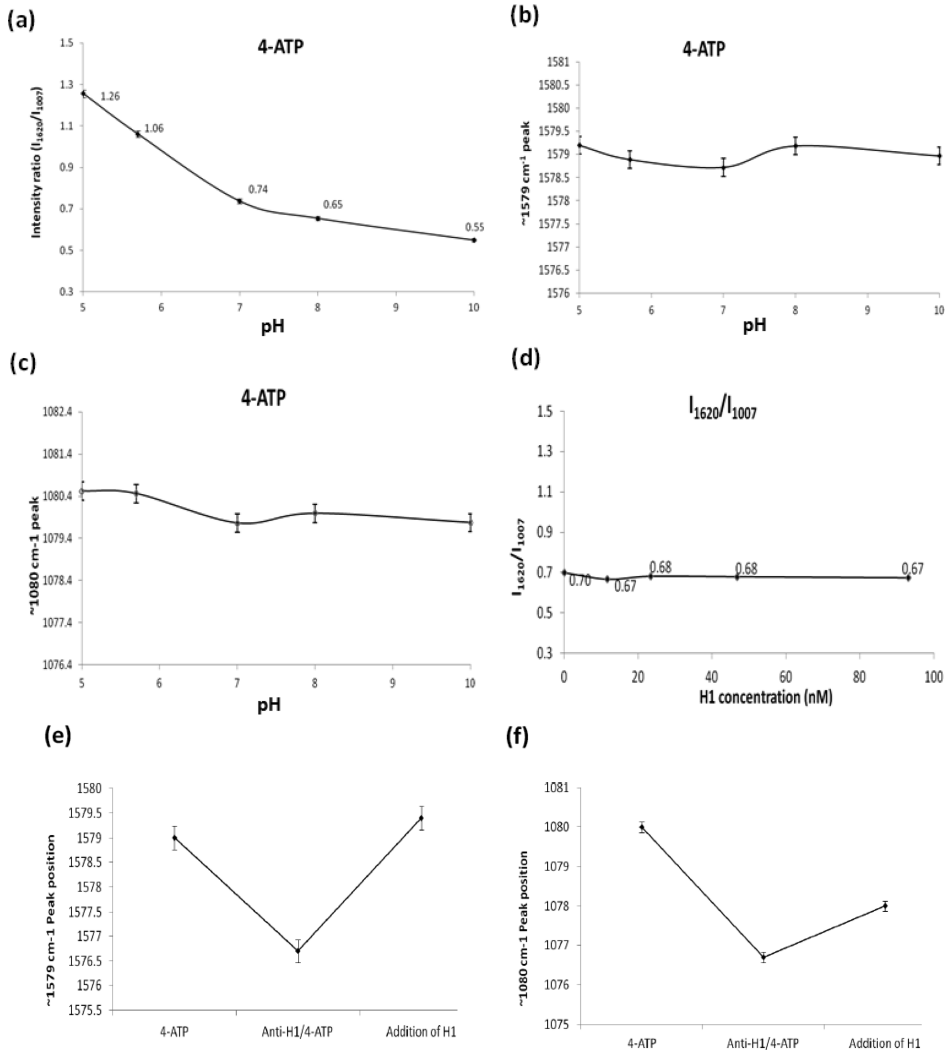

Figure 3. pH responses of 4-ATP. (a) pH response of intensity ratio I_{1620}/I_{1007} of a pure 4-ATP SAM. (b, c) Shifts in the 1580 cm^{-1} peak and 1080 cm^{-1} peak, respectively, derived from a pure 4-ATP SAM against pH changes. (d) Changes in the intensity ratio I_{1620}/I_{1007} of anti-H1/4-ATP against H1 concentrations. (e, f) Response of the 1580 cm^{-1} peak and 1080 cm^{-1} peak, respectively, to anti-H1 conjugation and H1−anti-H1 binding. Error bars = 0.02%.

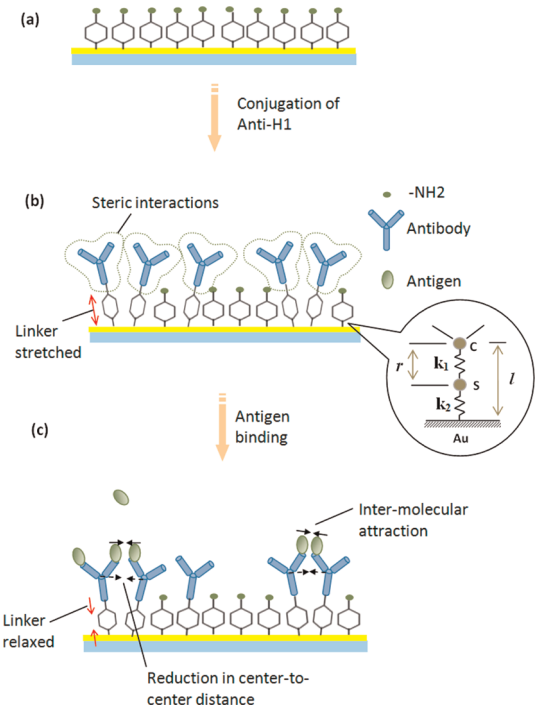

Figure 4. Mechanical deformation in an anti-H1/4-ATP sensor. (a) A pure 4-ATP SAM. (b) Conjugation of anti-H1 leads to stretching of the 4-ATP molecule. (c) Binding of H1 leads to reductions in the center-to-center distance between antibody molecules, thereby leading to mechanical relaxation in 4-ATP. Note that molecules shown are not drawn to scale. Inset: Mechanical model of the –C–S– bond.

deformation within the anti-H1-conjugated 4-ATP. For this purpose, we use the mechanical model of the C–S bond shown in Figure 4 as a demonstrative example. Assuming, for simplicity, equal spring constants, $k_1 = k_2 = k$, one can express changes in the spring length as $\Delta r = ((E'/E)^{1/2} - 1)r$, where E and E' are, respectively, the potential energies of each spring before and after being stretched (*i.e.*, before and after antibody conjugation) and r is the initial length of the spring before conjugation. In such a scenario, about 0.5% of the total binding energy (~334 kJ/mol) derived from the anti-H1-to-4-ATP conjugation is sufficient to induce a 0.23 pm (with r = 100 pm) extension in the C–S bond, which would correspond to a 2–8 cm^{-1} downshift in the Raman frequency,[27] as observed in our experiment.

Upon binding to the H1 antigen, however, the steric repulsion could be overcome by the attractive hydrophobic interactions between the bound antigens (Figure 4c), thereby causing the antigen–antibody complexes to pack slightly closer and relaxing the tensile deformation within the 4-ATP structure, which in turn upshifts both the 1080 and 1580 cm^{-1} peaks (see Figure 4c). Note that a reduced steric hindrance between antigen–antibody complexes is imaginable, given the fact that the antigen used (~53 kDa) is about 3 times smaller than the antibody (~150 kDa). In fact, mutual attractions between absorbent molecules

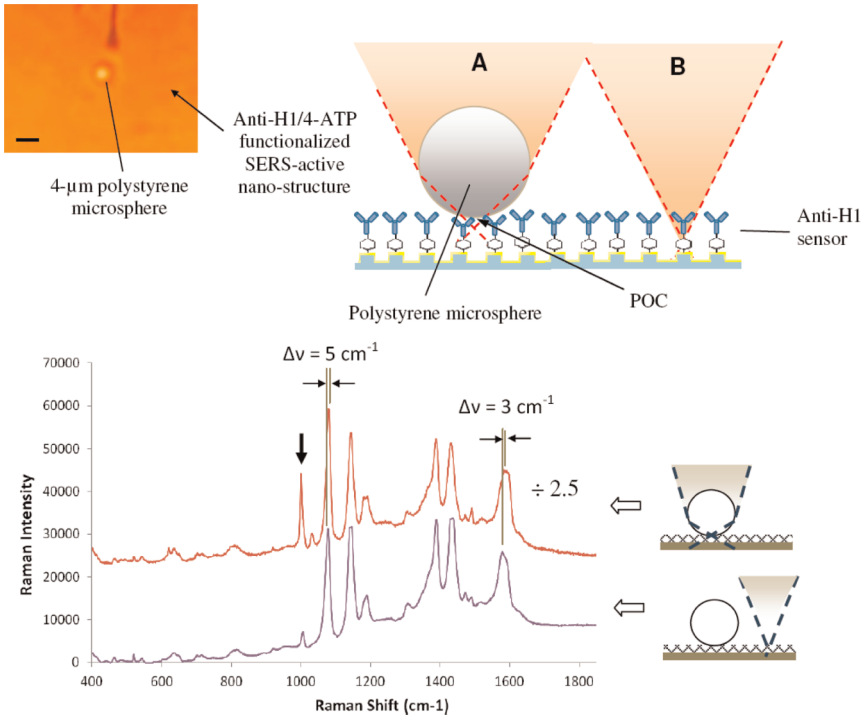

Figure 5. Pressure experiment with a 4 μm plain-surface polystyrene microsphere. Inset: Polystyrene microsphere on anti-H1/4-ATP-functionalized SERS-active nanostructure. Graph: SERS spectra measured from anti-H1/4-ATP with and without the bead. Note that the spectrum obtained through the bead has been scaled down by 2.5 times. Bar = 4 μm. Arrow indicates the 1000 cm^{-1} peak arising from the polystyrene bead.

have been observed previously on functionalized microcantilevers.[23,26,28]

To further ascertain our mechanical theory, we carried out another experiment in which a 4 μm plain-surface polystyrene microsphere was placed on the sensing surface (inset in Figure 5). This allows the weight of the microsphere to exert a downward mechanical pressure on the anti-H1/4-ATP layer at the point of contact (POC). Raman measurements were then performed with the laser beam focused at the POC through the microsphere, followed by another measurement with the sample slightly translated laterally (so the beam is no longer focused at the POC). The SERS spectra corresponding to the two beam positions are shown in Figure 5. Note that spectral intensities obtained through the bead are generally higher owing to the formation of an optical nanojet at the POC.[29] The peak at 1000 cm^{-1} (arrow in Figure 5) in the spectrum obtained from the POC is attributable to the polystyrene bead. It is observed that both the 1080 and 1580 cm^{-1} peaks are red-shifted by ~5 and 3 cm^{-1} when measured through the bead, which can be attributed to pressure forces exerted by the microsphere at the POC. Such a direct observation of pressure-induced shifts is significant, given the simplicity and convenience of the test. We subsequently repeated the experiment at various buffer pH's ranging between 5 and 10. Similar observations were again obtained, verifying that the peak shifts must be of a physical effect rather than a chemical one.

Demonstration of the Versatility of the Current Detection Scheme. Next, we demonstrate the versatility of our scheme by using a different linker molecule and a capturing antibody completely unrelated to the above one. In this second set of experiments, anti-p53 was chemically attached to 6-mercaptopurine (6-MP) *via* EDC/NHS coupling. In a similar manner to that above, SERS spectra were obtained for p53 concentrations ranging from 0 to 90 nM. Peak assignments are acquired from the reference Chu *et al.*[30] and shown in Table 3. Three peaks, situated at 865, 1000, and 1290 cm^{-1}, were found to be responsive to binding-induced stresses, in a fashion qualitatively describable by a first-absorption isotherm as shown in Figure 6d–f. The average detection limit in this case is estimated to be about 2.5 nM. The specificity test for anti-p53/6-MP sensor is shown in Figure 6g, with the 1290 cm^{-1} peak showing the highest distinguishability between p53 and BSA. For comparison, Figure 6h shows a dose–response curve for anti-p53 as obtained with a conventional ELISA. The DL for this particular assay is about 2.4 nM, with a saturation point at 20 nM.

Multiplexed Detection. Following the above studies, we subsequently ask whether multiplexed detection can be achieved in a mixed SAM of anti-H1/4-ATP and anti-p53/6-MP. Initial experiments carried out on mixed layers synthesized *via* coadsorption from a solution containing a mixture of anti-H1-conjugated 4-ATP and anti-p53-conjugated 6-MP failed to show antigen selectivity. A two-step fabrication method was later tried, in which the SERS substrate was first immersed in 100 nM 4-ATP solution prepared in ethanol for 1 h to form a submonolayer of 4-ATP. Subsequently, anti-H1 antibody was conjugated to the 4-ATP submonolayer *via* EDC/NHS. This is then followed by functionalization with anti-p53/6-MP complex. Figure 7a shows a typical composite SERS spectrum derived from the mixed SAM, in which peaks belonging to 4-ATP and 6-MP are clearly discernible. Detections of binding events in each type of sensor (anti-H1/4-ATP and anti-p53/6-MP) are illustrated in Figure 7b and c, whereby peak shifts at 1080 cm^{-1} in the composite spectrum are used for quantitating the bindings in the anti-H1/4-ATP sensor, while those at 1290 cm^{-1}, in the anti-p53/6-MP sensor. Note that two set of measurements were being carried out here, with each set using either H1- or p53-protein as the antigen. Also note that, for ease of comparison, fractional shifts, defined as the ratio of the binding-induced shift to the maximum achievable shift, are used. As can be seen, in each case, only the sensor specific to the antigen used produces the largest response, while responses in the other are suppressed, indicating some level of selectivity. To evaluate the amount of cross-talk between the anti-H1/4-ATP and the anti-p53/6-MP "channels", we defined percentage bleed-through as the percentage of the frequency shifts in a given sensor when presented with a nontargeted antigen, relative to the shifts attainable when presented with the targeted one. From the graphs, we calculate the percentage bleed-through at the maximum protein concentration (90 nM) to be 34% for the anti-H1/4-ATP and 16% for the anti-p53/6-MP. Although these values are significantly higher than the ideal value of 0%, the observation of binding selectivity in the mixed SAM is worthy of discussion. The fact that selectivity was attained in the SAMs prepared with the two-step fabrication

TABLE 3. Vibration Modes Observed by SERS Spectroscopy on a 6-MP Modified Nanostructure[a]

wavenumber (cm^{-1})	vibrational assignment
1572	δ(CH) + δ(CN) + δ(NH) + σ(CCN) + δ(NC)
1432	ν(CH) + ν(NH) + σ(NC) + ν(CC)
1382	δ(NH) + ν(CH) + ν(NH) + br(imid) + σ(CC)
1290	σ(NCC) + δ(NH) + δ(CH)
1214	ν(CH) + ν(NH) + σ(CS) + σ(NC)
1147	br(pyrim) + σ(CS) + δ(NH)
996	ν(CH) + ν(CNC) + ν(NH) + br(imid) + σ(CS) + δ(NC)
862	ν(CH)
787	tw(pyrim+imid) + δ(CH) + δ(NH)
689	br(pyrim) + δ(CS)
623	ν(NH) + σ(NC) + σ(CCC)

[a] ν: out-of-plane bending vibration; σ: stretching vibration; δ: in-plane vibration; br: ring breathing; tw: twisting vibration; pyrim: pyrimidine; imid: imidazole.

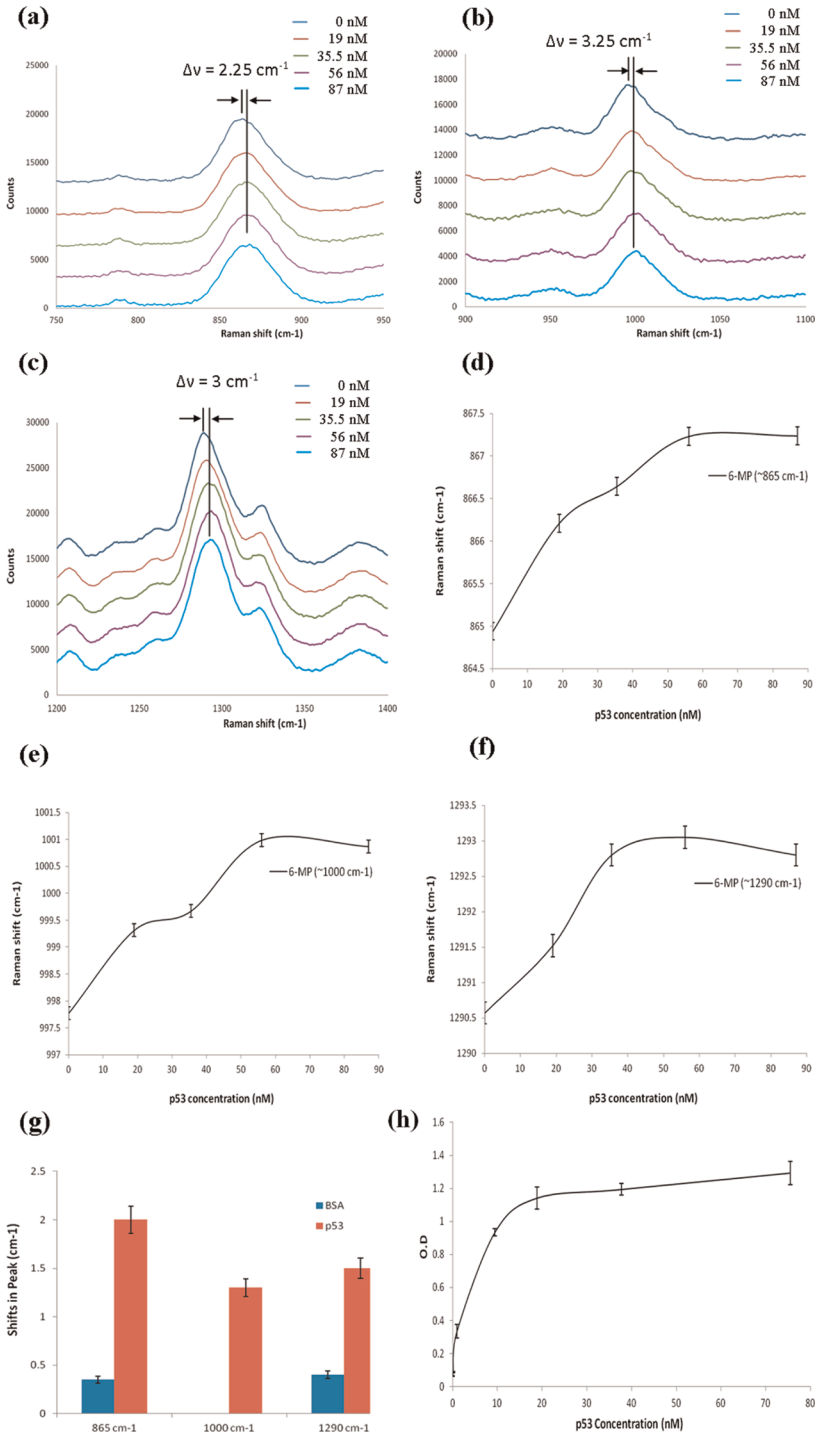

Figure 6. Responses of the anti-p53/6-MP to p53 concentrations. (a–c) Average SERS spectra at different p53 concentrations, showing shifts at 865, 1000, and 1290 cm^{-1}. (d–f) Response curve of SERS peaks at 865, 1000, and 1290 cm^{-1} to H1 concentrations. (g) Specific test showing selectivity of the three peaks. Error bars = 0.02%. (h) Dose–response curve for anti-p53 as obtained with ELISA. Note that, for clarity, SERS spectra shown in a–c have been offset vertically.

approach, as opposed to coabsorption from solution, suggests some degree of antibody segregations into separate nanodomains. We schematically illustrate this in Figure 7d. It is likely that the initial submonolayer of 4-ATP has self-organized into nanoislands, as observed previously,[31−33] leading to the anti-H1 self-assembled into domains upon conjugating to this 4-ATP layer. Subsequent functionalization with the anti-p53/6-MP complex then fills up the remaining unoccupied sites on the Au surface. This creates submicrometer regions of anti-H1/4-ATP and anti-p53/6-MP, between which binding events do not interfere, hence the selectivity. Nonetheless, we believe cross-talks between the anti-H1/4-ATP and the anti-p53/6-MP can be further

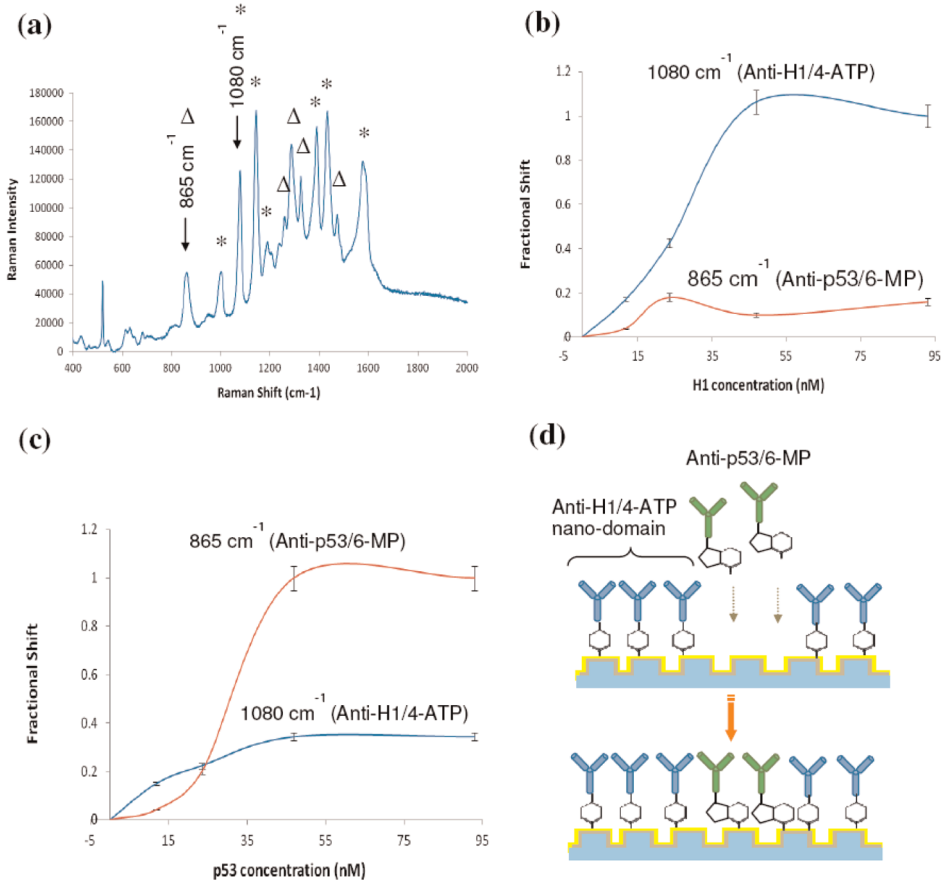

Figure 7. Multiplexed detection of H1 and p53 with a mixed SAM of anti-H1/4-ATP and anti-p53/6-MP. (a) Typical composite SERS spectrum derived from a mixed SAM of anti-H1/4-ATP (*) and anti-p53/6-MP (Δ). (b, c) Responses of the 865 and 1080 cm^{-1} peaks to different antigen (H1 and p53) concentrations. (d) Cartoon showing the compartmentalization of anti-H1/4-ATP and anti-p53/6-MP. Error bars = 5%.

improved through deterministic patterning with dip-pen nanolithography.[11] This shall be discussed in our future paper.

CONCLUSIONS

In this study, we showed that Raman-active purine as well as a phenol derivative can be used as SERS-active molecular nanostress sensors for the sensitive detection of proteins. We demonstrated that the vibration frequencies of antibody-conjugated SERS reporter molecules responded to the concentration of the targeted antigen in a quantitative fashion. Our stress sensors are found to exhibit a similar order of magnitude in detection limit as compared to conventional ELISA. Finally, we have demonstrated multiplexed subdiffraction measurements of two molecular sensors within one single laser spot. The detection limit of our sensor can be improved by optimizing the concentration of the Raman reporter SAM on a SERS substrate, and this will be considered in future studies. We anticipate that properly designed stress-sensitive and SERS-active reporters could lead to a novel way to detect binding events in submicrometer biofeatures, thereby bringing high-density protein sensing closer to reality.

EXPERIMENTAL SECTION

Materials. 4-Aminothiophenol, 1-ethyl-3-(3-dimethylaminopropyl) carbodiimide/*N*-hydroxysuccinimide, glycine, and bovine serum albumin were purchased from Sigma-Aldrich. Influenza A virus hemagglutinin H1 protein (H1, ab69741) and anti-H1 antibody (ab61986) were purchased from Abcam, while recombinant human p53 protein (556439) and anti-human p53 (554294) was purchased from BD Pharmingen.

Methods. *Fabrication of SERS-Active DUV Au/Ag Bimetallic Nanostructures.* The ordered and highly periodic nanogap arrays were fabricated on a Si wafer, according to previous reports.[34,35] Briefly, the fabrication process began with a deep UV photolithography transfer of the nanopattern onto a positive photoresist layer (410 nm thick and baked at 130 °C for 90 s) on the Si substrate. The gap size was adjusted by controlling the exposure dosages; a large exposure dosage would lead to smaller gap sizes. This is followed by silicon etching with SF_6 and C_4F_8 chemistry using an inductively coupled deep reactive ion etching system. Oxidation of the etched substrate was then performed at 900 °C between 2 and 6 h. Finally, the fabricated structures were first coated with an Ag layer (30 nm), followed by an Au layer (15 nm) using an e-beam evaporation system.

Functionlization of the SERS-Active DUV Au/Ag Bimetallic Nanostructures with an Anti-H1/4-ATP Layer. DUV Au/Ag

SERS-active substrates were cleaned thoroughly with ethanol. These substrates were then immersed in a 10 mM 4-ATP solution prepared in ethanol for 1 h. The substrates were then removed from the solution and washed thoroughly with ethanol to remove unbound 4-ATP, followed by rinsing with PBS. Anti-H1 solution was prepared by diluting 1 μL of anti-H1 stock (3.25 mg/mL) in 0.5 mL of PBS. The carboxyl terminal of the crystal segment of the antibody was activated by adding to the anti-H1 solution 5 μL of EDC/NHS (EDC = 171 mM/NHS = 427.5 mM) solution. The mixture was allowed to react for about 5 min. For anti-H1 conjugation, the 4-ATP-coated Au/Ag substrates were incubated in the mixture for 2 h at room temperature. Finally, the conjugated substrates were removed from the mixture and washed thoroughly with PBS. The substrates were then blocked with 1 mM EDC/NHS-activated glycine prepared in PBS for about 8 h. Upon completion of the incubation, the substrates were thoroughly washed with PBS.

Fabrication of Mixed SAM of Anti-H1/4-ATP and Anti-p53/6MP. DUV Au/Ag SERS-active substrates were cleaned thoroughly with ethanol. These substrates were then immersed in a 100 nM 4-ATP solution prepared in ethanol for 1 h to form a submonolayer of 4-ATP. The substrates were then removed from the solution and washed thoroughly with ethanol to remove unbound 4-ATP, followed by rinsing with PBS. Anti-H1 was then conjugated to the 4-ATP submonolayer in a similar manner as in §2 (SI). Anti-p53-conjugated 6-MP was prepared by mixing diluted anti-p53 solution (1 μL of anti-p53 stock (Pharmingen) in 0.5 mL of PBS) with 100 μM 6-MP. This is followed by activation with EDC/NHS (171 mM/427.5 mM) for 8 h at room temperature. The mixture was then applied onto the anti-H1/4-ATP-coated SERS-active substrate and reacted for 2 h at room temperature. Finally, the conjugated substrates were removed from the mixture and washed thoroughly with PBS. The substrates were then blocked with 0.1 mM EDC/NHS-activated glycine prepared in PBS for about 8 h. Upon completion of the incubation, the substrates were thoroughly washed with PBS.

Raman Measurements. Raman spectra were recorded with the entire substrate immersed in the H1 solution using a Renishaw inVia Raman microscope with 633 nm excitation wavelength at about 2 mW on the sample. Backscattered light was collected using a 50× objective lens with a 10 s integration time. Rayleigh scattering was blocked with a notch filter. For each H1 concentration, several scans were collected at various spots on the SERS-active region, and the acquired data were averaged. Background corrections and curve fittings of all SERS spectra were carried out using the Renishaw software, WiRE 2.0. All raw spectra were background subtracted by a 6-order polynomial fit before the curve-fitting procedure. All peaks were fitted by Gaussian curves to a tolerance of 0.01 based on an even weighting model.

Conflict of Interest: The authors declare no competing financial interest.

Acknowledgment. We would like to thank Mr. Zhi Qiang (attachment student from Nanyang Technological University, Singapore) for his help with Raman measurements. We also thank Dr. Ajay Agarwal (IME, A*STAR) for providing the substrates and Dr. Thoniyot (SBIC, A*STAR) for his assistance in this project.

Supporting Information Available: Additional information pertaining to the sensors is available free of charge *via* the Internet at http://pubs.acs.org.

REFERENCES AND NOTES

1. Richard, S. G.; Drew, A. H.; Shan, X. W. Autoassembly Protein Arrays for Analyzing Antibody Cross-Reactivity. *Nano Lett.* **2011**, *11*, 2579–2583.
2. Chen, C. S.; Mrksich, M.; Huang, S.; Whitesides, G. M.; Ingber, D. E. Geometric Control of Cell Life and Death. *Science* **1997**, *276*, 1425–1428.
3. Yue, M.; Stachowiak, J. C.; Lin, H.; Datar, R.; Cote, R.; Majumdar, A. Label-Free Protein Recognition Two-Dimensional Array Using Nanomechanical Sensors. *Nano Lett.* **2008**, *8*, 520–524.
4. Lockhart, D. J.; Winzeler, E. A. Genomics, Gene Expression and DNA Arrays. *Nature* **2000**, *405*, 827–836.
5. Chan, S. M.; Ermann, J.; Su, L.; Fathman, C. G.; Utz, P. J. Protein Microarrays for Multiplex Analysis of Signal Transduction Pathways. *Nat. Med.* **2004**, *10*, 1390–1396.
6. Ramachandran, N.; Raphael, J. V.; Hainsworth, E.; Demirkan, G.; Fuentes, M. G.; Rolfs, A.; Hu, Y.; LaBaer, J. Next Generation High Density Self-Assembling Functional Protein Arrays. *Nat. Methods* **2008**, *5*, 535–538.
7. Lee, K. B.; Kim, E. Y.; Mirkin, C. A.; Wolinsky, S. M. The Use of Nanoarrays for Highly Sensitive and Selective Detection of Human Immunodeficiency Virus Type 1 in Plasma. *Nano Lett.* **2004**, *4*, 1869–1872.
8. Demers, L. M.; S.Ginger, D.; Park, S. J.; Li, Z.; Chung, S. W.; Mirkin, C. A. Direct Patterning of Modified Oligonucleotides on Metals and Insulators by Dip-Pen Nanolithography. *Science* **2002**, *296*, 1836–1838.
9. Lynch, M.; Mosher, C.; Huff, J.; Nettikadan, S.; Johnson, J.; Henderson, E. Functional Protein Nanoarrays for Biomarker Profiling. *Proteomics* **2004**, *4*, 1695–1702.
10. Zhao, M.; Wang, X.; Nolte, D. Mass-Transport Limitations in Spot-Based Microarrays. *Biomed. Opt. Express* **2010**, *1*, 983–997.
11. Lee, K. B.; Lim, J. H.; Mirkin, C. A. Protein Nanostructures Formed *via* Direct-Write Dip-Pen Nanolithography. *J. Am. Chem. Soc.* **2003**, *125*, 5558–5589.
12. Martin, B. D.; Gaber, B. P.; Patterson, C. H.; Turner, D. C. Direct Protein Microarray Fabrication Using a Hydrogel "Stamper". *Langmuir* **1998**, *14*, 3971–3975.
13. Kumar, A.; Whitesides, G. M. Features of Gold Having Micrometer to Centimeter Dimensions Can be Formed Through a Combination of Stamping with an Elastomeric Stamp and an Alkanethiol "Ink" Followed by Chemical Etching. *Appl. Phys. Lett.* **1993**, *63*, 2002–2004.
14. Li, H. W.; Muir, B. V. O.; Fichet, G.; Huck, W. T. S. Nanocontact Printing: A Route to Sub-50 nm-Scale Chemical and Biological Patterning. *Langmuir* **2003**, *19*, 1963–1965.
15. Jaschke, M.; Butt, H. J. Deposition of Organic Material by the Tip of a Scanning Force Microscope. *Langmuir* **1995**, *11*, 1061–1064.
16. Fritz, J.; Baller, M. K.; Lang, H. P.; Rothuizen, H.; Vettiger, P.; Meyer, E.; Guntherodt, H. J.; Gerber, C.; Gimzewski, J. K. Translating Biomolecular Recognition into Nanomechanics. *Science* **2000**, *288*, 316–318.
17. Mayer, K. M.; Hafner, J. H. Localised Surface Plasmon Resonance Sensors. *Chem. Rev.* **2011**, *111*, 3828–3857.
18. Hong, S.; Lee, D.; Zhang, H.; Zhang, J. Q.; Resvick, J. N.; Khademhosseini, A.; King, M. R.; Langer, R.; Karp, J. M. Covalent Immobilization of P-selectin Enhanced Cell Rolling. *Langmuir* **2007**, *23*, 12261–12268.
19. Osawa, M.; Matsuda, N.; Yoshii, K.; Uchida, I. Charge Transfer Resonance Raman Process in Surface Enhanced Raman Scattering from P-Aminothiophenol Adsorbed on Silver: Herzberg-Teller Contribution. *J. Phys. Chem.* **1994**, *98*, 12702–12707.
20. Tseng, W. L.; Chang, H. T.; Hsu, S. M.; Chen, R. J.; Lin, S. Immunoaffinity Capillary Electrophoresis: Determination of Binding Constant and Stochiometry for Antibody-Antigen Interaction. *Electrophoresis* **2002**, *23*, 836–846.
21. Kho, K. W.; Shen, Z.; Olivo, M. Generation of Ultralarge Surface Enhanced Raman Spectroscopy (SERS)-Active Hot-Spot Volumes by an Array of 2D Nano-Superlenses. *Anal. Chem.* **2012**, *84*, 908–913.
22. Peica, N.; Lehene, C.; Leopold, N.; Schlucker, S.; Keifer, W. Monosodium Glutamate in Its Anhydrous and Monohydrate Form: Differentiation by Raman Spectroscopies and Density Functional Calculations. *Spectrochim. Acta A* **2007**, *66*, 604–615.
23. Moulin, A. M.; O'shea, S. J.; Badley, R. A.; Doyle, P.; Welland, E. E. Measuring Surface-Induced Conformational Changes in Proteins. *Langmuir* **1999**, *15*, 8776–8779.
24. Maiti, K. K.; Dinish, U. S.; Fu, C. Y.; Lee, J. J.; Soh, K. S.; Yun, S. W.; Bhuvaneswari, R.; Olivo, M.; Chang, Y. T. Development of Biocompatible SERS Nanotag with Increased

Stability by Chemisorption of Reporter Molecule for in Vivo Cancer Detection. *Biosens. Bioelectron.* **2010**, *26*, 398–403.
25. Kitagawa, T.; Tashiro, K.; Yabuki, K. Stress Distribution in Poly-p-Phenylenebenzobisoxazole (PBO) Fiber As Viewed from Vibrational Spectroscopic Measurement under Tension. I. Stress-Induced Frequency Shifts of Raman Bands and Molecular Deformation Mechanism. *J. Polym. Sci. Polym. Phys.* **2002**, *40*, 1269–1280.
26. Shu, W.; Laue, E. D.; Seshia, A. A. Investigation of Biotin-Streptavidin Binding Interactions Using Microcantilever Sensors. *Biosens. Bioelectron.* **2007**, *22*, 2003–2009.
27. Melendez, P. Y.; Ben, A. D. Intermolecular Forces and Bond Length Changes in High-Pressure Fluids. Vibrational Spectroscopic Measurement and Generalised Perturbed Hard Fluid Analysis. *J. Phys. Chem. B* **2000**, *104*, 7858–7866.
28. Tsouti, V.; Boutopoulos, C.; Andreakou, P.; Loannou, M.; Zergioti, I.; Goustouridis, D.; Kafetzopoulos, D.; Tsoukalas, D.; Normand, P.; Chatzandroulis, S. Detection of the Biotin-Streptavidin Interaction by Exploiting Surface Stress Changes on Ultrathin Si Membranes. *Microelectron. Eng.* **2009**, *86*, 1495–1498.
29. Lin, X.; Wang, X.; Liu, Z.; Ren, B. Enhanced Raman Scattering by Polystyrene Microspheres and Application for Detecting Molecules Adsorbed on Au Single Crystal Surface. *Acta Phys-Chim. Sin.* **2008**, *24*, 1941–1944.
30. Chu, H.; Yang, H.; Huan, S.; Shen, G.; Yu, R. Orientation of 6-Mercaptopurine SAMs at the Silver Electrode as Studied by Raman Mapping and In-Situ SERS. *J. Phys. Chem. B* **2006**, *110*, 5490–5497.
31. Mituso, K.; Tomoo, S.; Takumi, T.; Kazunori, T. Rapid Self-Assembly of Alkanethiol Monolayers on Sputter-Grown Au(111). *Langmuir* **2000**, *16*, 1719–1728.
32. Love, J. C.; Estroff, L. A.; Kriebel, J. K.; Nuzzo, R. G.; Whitesides, G. M. Self-Assembled Monolayers of Thiolates on Metals as a Form of Nanotechnology. *Chem. Rev.* **2005**, *105*, 1103–1169.
33. Tamada, K.; Nagasawa, J.; Nakanishi, F.; Abe, K. Structure and Growth of Hexyl Azobenzene Thiol SAMs on Au(111). *Langmuir* **1998**, *14*, 3264–3271.
34. Dinish, U. S.; Fu, C. Y.; Agarwal, A.; Olivo, M. Development of Highly Reproducible Nanogap SERS Substrates: Comparative Performance Analysis and Its Application for Glucose Sensing. *Biosens. Bioelectron.* **2011**, *26*, 1987–1992.
35. Tan, R. Z.; Agarwal, A.; Balasubramanian, N.; Kwong, D. L.; Jiang, Y.; Widjaja, E.; Garland, M. 3D Arrays of SERS Substrate for Ultrasensitive Molecular Detection. *Sens. Actuators, A* **2007**, *139*, 36–41.